Articles in PresS. Am J Physiol Lung Cell Mol Physiol (April 3, 2009). doi:10.1152/ajplung.00001.2009

THE INITIATION AND MATURATION OF CILIA GENERATED FLOW IN THE NEWBORN AND POSTNATAL MOUSE AIRWAY

Richard J.B. Francis[1], Bishwanath Chatterjee[1], Niki T Loges[2], Hanswalter Zentgraf[3], Heymut Omran[2], Cecilia W. Lo[1]†

[1]Laboratory of Developmental Biology, National Heart Lung and Blood Institute, National Institutes of Health, Bethesda, MD. [2]Department of Pediatrics and Adolescent Medicine, University Hospital Freiburg Mathildenstraße 1, D-79106 Freiburg, Germany.[3]Department of Tumor Virology, German Cancer Research Center, D-69120 Heidelberg, Germany.

Running head: Cilia flow in neonate mouse trachea

† Corresponding Author:

10 Center Drive,

Building 10/Room 6C-103A,

MSC-1583, Bethesda,

MD 20892.

Phone: 301-451-8041.

FAX: 301-480-4581.

Email: loc@nhlbi.nih.gov

"The costs of publication of this article were defrayed in part by the payment of page charges. The article must therefore be hereby marked 'advertisement' in accordance with 18 U.S.C. Section 1734 solely to indicate this fact."

ABSTRACT:

Mucociliary clearance in the adult trachea is well characterized, but there is limited data in newborns. Cilia generated flow was quantified across longitudinal sections of mouse tracheal from birth through postnatal day (PND) 28 by tracking fluorescent microsphere speed and directionality. The percentage of ciliated tracheal epithelial cells, as determined by immunohistochemistry, was shown to increase linearly between PND 0-21 (R^2=0.94). While directionality measurements detected patches of flow starting at PND 3, uniform flow across the epithelia was not observed until PND 7 at a ~35% ciliated cell density. Flow became established at a maximal rate at PND 9 and beyond. A linear correlation was observed between the percentage of ciliated cells versus flow speed (R^2=0.495) and directionality (R^2=0.975) between PND 0-9. Cilia beat frequency (CBF) was higher at PND 0 than all subsequent time points, but cilia beat waveform was not noticeably different. Tracheal epithelia from a mouse model of PCD harboring a *Mdnah5* mutation showed ciliated cell density was unaffected, but no cilia generated flow was detected. Cilia in mutant airways were either immotile, or with slow dyssynchronous beat and abnormal ciliary waveform. Overall, our studies showed the initiation of cilia generated flow is directly correlated with an increase in epithelial ciliation, with the measurement of directionality being more sensitive than speed for detecting flow. The higher CBF observed in newborn epithelia suggests unique physiology in the newborn trachea, indicating possible clinical relevance to the pathophysiology of respiratory distress seen in newborn PCD patients.

Key words: ciliogenesis, development, murine, primary ciliary dyskinesia, cilia, trachea

INTRODUCTION

Cilia associated defects are becoming increasingly recognized as playing pivotal roles in a diverse array of pathophysiological processes referred to as ciliopathies (for reviews see (3, 8)). During embryonic development, motile cilia in the node generate nodal flow required for the specification of left-right asymmetry, with disruption or loss of this flow causing defects in laterality (Review: (26)) (12, 15, 30). Motile cilia also are important in maintaining normal brain, lung, and reproductive function, as defects in cilia motility can also cause hydrocephalus (12, 13, 15, 16, 29), chronic respiratory disease (21, 28), and infertility (20), respectively.

Primary ciliary dyskinesia (PCD) (MIM#242650) is a rare disorder, usually inherited as an autosomal recessive trait. It affects approximately 1 in 20,000 individuals, and is characterized by inborn defects of cilia motility (28). PCD patients often suffer from chronic destructive airway disease due to reduced airway cleaning caused by reduced mucociliary clearance. Approximately half of the affected individuals exhibit situs inversus, presumably due to randomization of left/right body asymmetry caused by defects associated with motile cilia at the embryonic node. The association of situs inversus and PCD is also referred to as Kartagener's syndrome. Many PCD patients present as neonates with postnatal respiratory distress, which is often misdiagnosed as neonatal pneumonia (28). Interestingly, so far no studies have systematically addressed function of respiratory cilia in neonates.

In the context of a large scale mouse mutagenesis screen for mutations causing congenital heart disease (33), we recovered several mutant mouse models with phenotypes linked to defects in motile and non-motile cilia, such as heterotaxy and other

laterality defects, hydrocephalus, kidney cysts and cysts in other organs ((2, 30, 33), unpublished observations). To evaluate for disruption of cilia motility in these mutants, we assessed ciliary function in the tracheal epithelia as a proxy for motile cilia in the embryonic node or ependymal cilia in the brain (30). Given many of our mutant mice do not survive long term postnatally due to the severe structural heart defects, the cilia assessments are largely conducted using the airway of neonates or young pups. In contrast to the well described cilia dynamics and cilia generated flow in the adult mouse trachea, no information is available on motile cilia function in neonatal mouse trachea (4, 19, 22, 32). Thus the aim of this study is to characterize ciliary motion and cilia generated flow in the mouse trachea during normal neonatal and early postnatal development.

We examined the emergence of ciliated cells in the airway epithelia in mice from postnatal day (PND) 0 to 28, and measured ciliary beat frequency and waveform using video microscopy. Net flow across the epithelia was evaluated by quantitating directionality and speed associated with the movement of fluorescent beads placed in the medium surrounding the tracheal epithelia. We found directionality measurements were more sensitive than speed for detecting cilia generated flow, with directionality measurements detecting patches of flow as early as PND 3, while speed measurements failed to detect flow until PND 7. Overall, flow was observed to become established between PND 5-7 with a epithelial ciliated cell density 30-35%, and reached a maximal flow state at PND 9 and beyond. Interestingly, ciliary beat frequency (CBF) was highest just after birth, possibly an indication of unique physiology associated with the newborn trachea. Using these same approaches, we analyzed ciliary function in an established

mouse model of PCD, and showed reduced CBF with a shortened stroke and abnormal ciliary waveform (30).

MATERIALS AND METHODS

Mouse breeding and trachea collection.

Experiments were conducted in accordance with an approved animal protocol of the National Heart Lung Blood Institute (Protocol Number H-0175) using C57BL/6 mice 0-28 postnatal days (PND) in age. After euthanasia, trachea were removed in L-15 media +10% fetal bovine serum (Invitrogen, CA), and cut longitudinally and either immediately fixed for immunohistochemistry, or transferred into a dish for video microscopy.

Immunohistochemistry

For immunostaining, tracheas were fixed in 4% paraformaldehyde then secured to a glass coverslip with the tissue adhesive Nexaband® (Webster Veterinary, MA), then permeabilized with PBST (0.2% Triton X-100 in PBS), blocked with 5% goat serum, and incubated overnight at 4°C with a anti-α-tubulin antibody (Sigma, MO). Secondary fluorescent labeling used the anti-mouse Cy3 antibody (Jackson ImmunoResearch Laboratories, PA) diluted in PBST containing Alexa Fluor® 488 conjugated phalloidin (5 ul/200 ul; Invitrogen, CA). The tissue was imaged using a Leica DMLFSA microscope with a 63x water immersion objective and Hamamatsu ORCA-ER digital CCD camera. 3-4 areas (150µm x 200µm) were imaged at random along the length of each trachea (n=5-6 trachea per time-point) and Z-stacks were collected using GFP and Cy3 filter sets and OpenLab 3.1.7 software (Improvision, UK). Each Z-stack was volume deconvoluted and collapsed into a single colour image, with the GFP and Cy3 images merged for counting ciliated vs non-ciliated cells. Mdnah5 staining was conducted as described above on air dried trachea scrapes using a mouse monoclonal and rabbit polyclonal produced against the human DNAH5 protein (to amino acid residues 42-325 of DNAH5)

(9, 24).

Quantitation of trachea ciliary motility and ciliary generated flow by video microscopy

Trachea strips were secured luminal side down on a 35mm glass bottomed culture dish (Willco Wells B.V, Netherlands) using a glass coverslip covered with a silicone sheet containing a small window to form a chamber. Cilia dynamics were captured along the edge of the trachea strips at room temperature using a 100x DIC oil objective and Leica inverted microscope (Leica DMIRE2), and movies (200 fps) made using a Phantom v4.2 camera (Vision Research, NJ). To quantify ciliary beat frequencies, the number of frames required for completion of a single stroke were counted. To quantify flow, 0.20μm Fluoresbrite microspheres (Polysciences, PA) were added to the trachea bathing media, and fluorescent movies (15 fps) were collected using FITC filter prisms and high-speed CCD camera (Hamamatsu, C9100-12). Microsphere speed and directionality were obtained from the movies using Volocity 3.5.1 software (Improvision, UK). For measuring both cilia dynamics and cilia generated flow 3-4 randomly selected areas were imaged from 5-6 trachea per developmental time-point, from which up to 8 microspheres were tracked per area. Directionality was defined as the net displacement achieved (ie. the straight line connecting microsphere location in time-point 0 to the last time-point measured) divided by the total distance traveled (ie. the zig-zag line collected by tracing microsphere location across all time-points); thus a microsphere moving in a straight line would have a directionality of one, while more random movements approach a directionality of zero.

Immunoblotting

Tracheas were dissected and homogenized (Polytron PT1200) in buffer containing 5 mM PMSF and 1% NP40, centrifuged at 12,000Xg for 10 minutes at 4°C. The supernatant was then separated on NuPAGE 3-8% Tris-acetate gel (Invitrogen, Karlsruhe, Germany) and blotted onto a PVDF membrane (Amersham). Immunodetection was carried out using ECL plus (GE Healthcare, Germany), with monoclonal and polyclonal anti-DNAH5 made to amino acid residues 42-325 (9, 24).

Data analysis

Data is presented as mean ± SD as analyzed using Instat 3 (GraphPad Software, Inc.) with one-way analysis of variance (ANOVA) and Bonferroni post-test for comparison of all time-points. Graphs and linear fit lines were generated/analyzed using Prism 5 (GraphPad Software, Inc.), with the F test used to determine if slopes were significantly different than zero.

RESULTS.

i) Emergence of ciliated epithelial cells in the trachea

Ciliated cells in the mouse tracheal epithelium from birth to PND 28 were visualized using an anti-α-tubulin antibody in conjunction with a fluorochrome conjugated secondary antibody. Newborn trachea contained few ciliated cells (Fig 1A), but the ciliated epithelial cell density steadily increased with postnatal development (Fig 1A-F). To quantitate the emergence of ciliated cells, fluorochrome conjugated phalloidin was used to delineate cell borders in the epithelia, and the percentage of ciliated cells was calculated from the ratio of ciliated cells over total epithelial cells observed per image field. This showed the density of ciliated cells in the trachea increased linearly following birth, plateauing at PND 14 (Fig 1G). A positive linear correlation (R^2=0.94, P=0.0003) was observed between the percentage of ciliated cells and postnatal development from birth up to PND 21 (Fig 1G).

ii) Analysis of Tracheal Flow.

To quantify cilia generated flow, we used videomicroscopy with epifluorescent illumination to visualize the movement of fluorescent microspheres placed in the culture media bathing the trachea. Digital images were captured at 15 fps to track the movement of individual beads. In newborn tracheal epithelia, the beads did not display coordinated directional movement (Fig 2C, see Movie E1 in the online data supplement), but instead exhibited only random Brownian motion (traces in Fig 2C). Consequently, no net flow was observed. In contrast, similar analysis of PND 14 trachea showed coordinated or directional movement of the beads, with net flow of the beads observed across the tracheal epithelia (traces in Fig 2D, see Movie E2 in the online data supplement).

Quantitation of microsphere motion showed a biphasic distribution for microsphere speed and directionality (Fig 2E-F). Microsphere speed was unchanged from PND 0-5, followed by a significant increase at PND 7, with a new plateau reached at PND 9 onwards (Fig 2E). Microsphere directionality displayed a similar developmental profile to that of speed, but was shifted earlier by approximately 3 days (Fig 2F), with a low plateau 0-3 days after birth, a significant increase at PND 5, with a new plateau reached at PND 7 and onwards (Fig 2F).

Examination of speed and directionality histograms revealed PND 0 microsphere motion (Fig 3A,B) was identical to that observed in control experiments where microspheres were placed in medium without any tracheal samples (data not shown). This confirms that the motion observed at PND 0 corresponds to Brownian motion. Speed histograms (Fig 3) showed a broadening distribution differing from Brownian motion starting at PND 7 (Fig 3G), as flow across the epithelia became established. In contrast, histogram distribution for directionality measurements was already right shifted at PND 3 (Fig. 3D). This corresponds to the emergence of patches of flow in the tracheal epithelia. These results show flow directionality is more sensitive then flow speed measurements for the detection of cilia generated flow.

iii) Analysis of cilia waveform and beat frequency.

Longitudinal trachea sections used to visualize microsphere motion using epifluorescent illumination were also imaged using standard DIC imaging. This allowed the visualization of ciliary waveform and the quantitation of cilia beat frequency (CBF) with images captured at 200 fps using a high speed camera (Fig. 4, see Movie E3 in the online data supplement). Tracing of cilia beat shape from images obtained from

individual ciliated cells at PND 0 (Fig. 4A, C-D) and PND 14 (Fig. 4B, E-F) showed no difference in their cilia waveforms. Quantitation of CBF showed that while the CBF in E18.5 embryos and PND 1-2 stage neonates was moderately elevated compared with later stages, there was a significant spike in CBF at birth (PND 0). This was significantly higher compared to all other time points - being 23.4 ± 4.4 Hz at birth, then rapidly declining to reach a plateau of 13.6 ± 3.4 Hz at PND 3 onwards (Fig. 4G).

iv) Cilia generated flow correlates with increase in ciliated cell density.

Our finding that cilia generated flow in the tracheal epithelia increased with postnatal developmental age is consistent with the increase in the density of ciliated cells in the tracheal epithelia. To determine whether the density of ciliated cells in the epithelia is directly correlated with flow, we plotted percent ciliated cells vs. flow speed or flow directionality at PND 0-28 (red lines in Fig 5) or PND 0-9 (green lines in Fig 5). Between PND 0-20, a positive linear correlation was observed between percent ciliated cells vs. flow speed or directionality (R^2=0.743, P=0.006 for speed; R^2=0.807, P=0.002 for directionality) (see red lines in Fig 5A,B). However, between PND 0-9 when cilia generated flow is being established, the correlation of ciliated cell density with speed was weaker (R^2=0.495, P=0.185), while the correlation with directionality was the strongest (R^2=0.975, P=0.002) (see green lines in Fig 5A,B). These results further show directionality rather than speed is a more sensitive parameter for assessing cilia generated flow. The plot of directionality vs. percent ciliated cells show maximal directionality of 1 is achieved at 35% ciliated cell density, indicating this is the critical ciliated cell density required for uniform flow across the airway epithelia (Fig 5B).

v) Abnormal ciliary waveform and no flow in PCD mouse model

Using the flow criteria established in the studies above, we examined tracheal epithelia in a mouse model of PCD with a mutation in *Mdnah5* (alias *Dnahc5*), the ortholog of human DNAH5 - the gene most commonly mutated in patients with PCD (11). This mutation, $Mdnah5^{del267\text{-}859}$, causes an in-frame deletion of 593 amino acids (residues 267 to 859) which does not include the dynein motor domain in Mdnah5 (30). Homozygous $Mdnah5^{del267\text{-}859}$ mice can survive postnatally up to four weeks of age, eventually expiring due to hydrocephalus (30). We previously showed this mutation caused an outer dynein arm defect, which is also commonly observed in PCD patients with *DNAH5* mutations (28).

To better understand the molecular perturbation that underlie the outer dynein arm defect in $Mdnah5^{del267\text{-}859}$ mutant mice, we performed immunostaining with monoclonal and polyclonal antibodies directed against the N-terminus (residues 42-328) of human DNAH5 protein. We first demonstrated cross-species specificity of the antibodies by Western blot analyses, which yielded in cell lysates of mouse tracheal epithelia a specific ~500 kD band, the size range expected for full length Mdnah5 protein (Fig. 6A,C). High-resolution immunofluorescence analyses revealed that in control cells, Mdnah5 is specifically expressed in the ciliary axonemes of airway epithelial cells (Fig. 6B,D). In the homozygous $Mdnah5^{del267\text{-}859}$ mutant, only low background staining was observed in the ciliary axoneme (Fig. 6B,D). This is consistent with previous findings in respiratory cells from PCD patients harboring various recessive loss-of-function *DNAH5* mutations (9). We note the staining observed in the apical cytoplasm in the area of the microtubules organizing centers or basal bodies also has been observed in respiratory cells of PCD

patients with DNAH5 mutations (11). This might reflect abnormal trafficking of mutant DNAH5/Mdnah5 protein or some nonspecific staining.

Videomicroscopy of the tracheal epithelia from PND 3 to 28 showed the cilia in these mutants as either immotile, or with slow dyssynchronous beat (see Movie E4 in the online data supplement). Examination of the ciliated cell density showed the percentage of ciliated tracheal cells in homozygous *Mdnah5*$^{del267-859}$ mutants was not different from their wildtype littermates (data not shown), but the cilia that were motile displayed a significantly reduced CBF when compared to that of wildtype littermates (1.7 ± 1.6 vs 14.4 ± 4.4 Hz). Quantitation of flow directionality and speed across the trachea of these mutants using fluorescent microspheres showed no evidence of flow at any postnatal developmental time-points examined (see Movie E5 in the online data supplement) (Fig. 6E, F). Analysis of ciliary motion associated with motile cilia in the mutant epithelia revealed abnormal ciliary waveform with a shortened stroke (Fig 6G) (see Movie E4 in the online data supplement).

DISCUSSION.

Our studies show mice are born with few ciliated tracheal epithelia cells and ex vivo analysis of isolated trachea showed no discernable cilia generated flow across the tracheal epithelia. Ciliated cell abundance increased linearly following birth, reaching a plateau at PND 14. The progressive increase in epithelial ciliation of the neonatal mouse trachea closely matched the findings of Toskala et al. (31). They showed cilia first appeared in trachea at embryonic day 16 and increased until PND 14-21. However, this previous study did not include functional analysis of ciliary motion or cilia generated flow (31).

Our assessment of cilia generated flow using fluorescent microspheres showed an increase in flow concurrent with increase in abundance of ciliated cells in the tracheal epithelia. Microsphere speed and directionality measurements exhibited a biphasic distribution, with no flow observed at birth, followed by the rapid initiation of flow between PND 5-7, and rising to a plateau at PND 9. We found that histograms of speed and directionality measurements better described the patchy nature of flow observed across the tracheal epithelia. Flow directionality measurements showed patches of flow as early as PND 3, although they were outnumbered by many areas of non-flow. The ratio increased in favor of flow vs. non-flow patches such that by PND 7, flow was observed uniformly across the entire epithelia in all trachea analyzed. In contrast to flow directionality, histogram of flow speed measurements did not detect flow until PND 7.

We found the initiation of cilia generated flow was directly correlated with the increase in ciliated cell density, with microsphere directionality rather than speed showing the best correlation. These findings further show flow directionality is a more

sensitive parameter for assessing flow. This reflects the fact that Brownian motion would mask flow at low speeds, which might nevertheless be detectable with the examination of flow directionality. While a number of cilia array studies have previously examined the ability of cilia to generate fluid flow (10, 18), our studies identified that the ~35% ciliated cell density associated with the PND 7 tracheal epithelia is the critical ciliation density required to generate uniform epithelial flow. Although we only examined the tracheal epithelia, our findings is likely to be relevant for flow in the bronchi and bronchioli, as anatomical observations show ciliated cell density in these airway structures increased in a manner similar to that of the trachea (31). However, as the trachea airway *in vivo* is coated with a thin layer of higher viscosity mucus, further studies of cilia mediated flow using more viscous medium are needed to evaluate how changes in the density of epithelial ciliation may affect mucociliary clearance.

Our findings that cilia generated flow in the tracheal epithelia emerges over a period of days postnatally led us to reexamine ciliary function in the *Mdnah5*$^{del267\text{-}859}$ mutant mouse model of PCD (30). Using videomicroscopy, we previously showed no detectable cilia generated flow in *Mdnah5*$^{del267\text{-}859}$ mutants, although some ciliary motion was observed (30). In this study, we showed there is no change in the density of epithelial ciliation in the mutant tracheal epithelia. Examination of ciliary motion revealed slow dyskinetic movement, with an abnormal ciliary waveform. The cilia beat failed to exhibit the full stroke seen in normal airway cilia motion. Analysis using fluorescent beads showed no net flow generated by the dyssynchronous ciliary beat associated with the mutant airway epithelia. Immunostaining with a DNAH5 antibody

suggested the mutant *Mdnah5* protein, though expressed, is not transported to the ciliary axoneme.

Airway cilia have proved useful as a experimental paradigm to assess the functional roles served by genes known or suspected to be encode proteins in the ciliome (12, 16, 17, 29). Our results suggest measuring cilia generated flow to assess the potential physiological function of genes in the ciliome would not be possible in mutant mice that die prenatally or neonatally. In such instances, using FOXJ1-Cre (34) with the cre/lox system (25) could be used to delete the genes of interest specifically in the tracheal epithelia, thereby rescuing the prenatal/neonatal lethality.

The lack of cilia generated flow in newborn tracheas is not due to altered cilia waveform, as our analysis showed newborn trachea have ciliary waveform or stroke similar to that seen in normal adult mouse airway (16). Rather, the lack of flow is a reflection of the low ciliation cell density in the newborn trachea. While our CBF measurements from PND 3 onwards were similar to that of the CBF found in adult mouse airway (4, 6, 17, 29), an unexpected elevation of CBF was seen in the early mouse neonate which peaked at birth. The finding of elevated CBF in the newborn trachea may represent a higher primitive autonomous CBF displayed by isolated ciliated cells before establishment of metachronal coordination characteristic of mature airway epithelia(27), an idea reminiscent of the autonomous pacemaker activity of isolated myocytes. An alternative explanation is that the sharp CBF peak seen at birth is due to shear stress with fluid clearance and/or perfusion of air into the lungs. Although our data suggest the airway epithelia of newborn mice are too sparsely ciliated to generate flow, it is interesting to note that human neonates with PCD often develop respiratory distress (7).

Thus studies are warranted to assess CBF and ciliation density in the human newborn airway epithelia to ascertain the potential role of cilia generated flow in the clearance of amniotic fluid from the lungs and its possible contribution to the pathophysiology of neonatal respiratory distress. We note that although clinical studies measuring CBF from nasal biopsies in human subjects have largely not shown any change in CBF with age (1, 5, 14), the youngest infants examined were 5 days old (23).

In conclusion, *ex vivo* analysis of mouse tracheal epithelia showed cilia generated flow is initiated between PND 5-7, becoming established with maximal flow at PND 9. This is correlated with a linear increase in the density of ciliated tracheal epithelia cells, with ~35% ciliation required for uniform flow epithelia flow. Our study demonstrates that the most effective use of microspheres for monitoring flow is the measurement of flow directionality rather than speed. Further investigation is needed to examine the efficacy of mucociliary clearance as epithelial ciliation increases with postnatal development. Whether the high CBF observed in newborn mice may have clinical relevance will require further investigation of ciliary density and function in human newborns. Overall, these findings should prove useful for investigating the pathophysiology of ciliopathies involving the airway.

ACKNOWLEDGMENTS

This work was supported by NIH grant ZO1-HL-005701.

REFERENCES

1. **Ahmad I and Drake-Lee A.** Nasal ciliary studies in children with chronic respiratory tract symptoms. *Rhinology* 41: 69-71, 2003.
2. **Aune CN, Chatterjee B, Zhao XQ, Francis R, Bracero L, Yu Q, Rosenthal J, Leatherbury L, and Lo CW.** Mouse model of heterotaxy with single ventricle spectrum of cardiac anomalies. *Pediatric Research* 63: 9-14, 2008.
3. **Badano JL, Mitsuma N, Beales PL, and Katsanis N.** The ciliopathies: an emerging class of human genetic disorders. *Annual Review of Genomics & Human Genetics* 7: 125-148, 2006.
4. **Delamanche S, Desforges P, Morio S, Fuche C, and Calvet JH.** Effect of oleoresin capsicum (OC) and ortho-chlorobenzylidene malononitrile (CS) on ciliary beat frequency. *Toxicology* 165: 79-85, 2001.
5. **Edwards EA, Douglas C, Broome S, Kolbe J, Jensen CG, Dewar A, Bush A, and Byrnes CA.** Nitric oxide levels and ciliary beat frequency in indigenous New Zealand children. *Pediatric Pulmonology* 39: 238-246, 2005.
6. **Elliott MK, Sisson JH, and Wyatt TA.** Effects of cigarette smoke and alcohol on ciliated tracheal epithelium and inflammatory cell recruitment. *American Journal of Respiratory Cell & Molecular Biology* 36: 452-459, 2007.
7. **Ferkol T and Leigh M.** Primary ciliary dyskinesia and newborn respiratory distress. *Seminars in Perinatology* 30: 335-340, 2006.
8. **Fliegauf M, Benzing T, and Omran H.** When cilia go bad: cilia defects and ciliopathies. *Nature Reviews Molecular Cell Biology* 8: 880-893, 2007.
9. **Fliegauf M, Olbrich H, Horvath J, Wildhaber JH, Zariwala MA, Kennedy M, Knowles MR, and Omran H.** Mislocalization of DNAH5 and DNAH9 in respiratory cells from patients with primary ciliary dyskinesia. *American Journal of Respiratory & Critical Care Medicine* 171: 1343-1349, 2005.
10. **Guirao B and Joanny JF.** Spontaneous creation of macroscopic flow and metachronal waves in an array of cilia. *Biophysical Journal* 92: 1900-1917, 2007.
11. **Hornef N, Olbrich H, Horvath J, Zariwala MA, Fliegauf M, Loges NT, Wildhaber J, Noone PG, Kennedy M, Antonarakis SE, Blouin JL, Bartoloni L, Nusslein T, Ahrens P, Griese M, Kuhl H, Sudbrak R, Knowles MR, Reinhardt R, and Omran H.** DNAH5 mutations are a common cause of primary ciliary dyskinesia with outer dynein arm defects.[see comment]. *American Journal of Respiratory & Critical Care Medicine* 174: 120-126, 2006.
12. **Ibanez-Tallon I, Gorokhova S, and Heintz N.** Loss of function of axonemal dynein Mdnah5 causes primary ciliary dyskinesia and hydrocephalus. *Human Molecular Genetics* 11: 715-721, 2002.
13. **Ibanez-Tallon I, Pagenstecher A, Fliegauf M, Olbrich H, Kispert A, Ketelsen UP, North A, Heintz N, and Omran H.** Dysfunction of axonemal dynein heavy chain Mdnah5 inhibits ependymal flow and reveals a novel mechanism for hydrocephalus formation. *Human Molecular Genetics* 13: 2133-2141, 2004.
14. **Jorissen M, Willems T, and Van der Schueren B.** Nasal ciliary beat frequency is age independent. *Laryngoscope* 108: 1042-1047, 1998.
15. **Kennedy MP, Omran H, Leigh MW, Dell S, Morgan L, Molina PL, Robinson BV, Minnix SL, Olbrich H, Severin T, Ahrens P, Lange L, Morillas HN, Noone PG,**

Zariwala MA, and Knowles MR. Congenital heart disease and other heterotaxic defects in a large cohort of patients with primary ciliary dyskinesia.[see comment]. *Circulation* 115: 2814-2821, 2007.

16. **Lechtreck KF, Delmotte P, Robinson ML, Sanderson MJ, and Witman GB.** Mutations in Hydin impair ciliary motility in mice. *Journal of Cell Biology* 180: 633-643, 2008.

17. **Lee L, Campagna DR, Pinkus JL, Mulhern H, Wyatt TA, Sisson JH, Pavlik JA, Pinkus GS, and Fleming MD.** Primary ciliary dyskinesia in mice lacking the novel ciliary protein Pcdp1. *Molecular & Cellular Biology* 28: 949-957, 2008.

18. **Lenz P and Ryskin A.** Collective effects in ciliar arrays. *Physical Biology* 3: 285-294, 2006.

19. **Look DC, Walter MJ, Williamson MR, Pang L, You Y, Sreshta JN, Johnson JE, Zander DS, and Brody SL.** Effects of paramyxoviral infection on airway epithelial cell Foxj1 expression, ciliogenesis, and mucociliary function. *American Journal of Pathology* 159: 2055-2069, 2001.

20. **Lyons RA, Saridogan E, and Djahanbakhch O.** The reproductive significance of human Fallopian tube cilia. *Human Reproduction Update* 12: 363-372, 2006.

21. **Mall MA.** Role of cilia, mucus, and airway surface liquid in mucociliary dysfunction: lessons from mouse models. *Journal of aerosol medicine & pulmonary drug delivery* 21: 13-24, 2008.

22. **Matsubara E, Nakahari T, Yoshida H, Kuroiwa T, Harada KH, Inoue K, and Koizumi A.** Effects of perfluorooctane sulfonate on tracheal ciliary beating frequency in mice. *Toxicology* 236: 190-198, 2007.

23. **O'Callaghan C, Smith K, Wilkinson M, Morgan D, and Priftis K.** Ciliary beat frequency in newborn infants. *Archives of Disease in Childhood* 66: 443-444, 1991.

24. **Omran H, Kobayashi D, Olbrich H, Tsukahara T, Loges N, Hagiwara H, Zhang Q, Leblond G, O'Toole E, Hara C, Mizuno H, Kawano H, Fliegauf M, Yagi T, Koshida S, Miyawaki A, Zentgraf H, Seithe H, Reinhardt R, Watanabe Y, Kamiya R, Mitchell D, and Takeda H.** Ktu/PF13 is required for cytoplasmic pre-assembly of axonemal dynein. *Nature (in press)*, 2008.

25. **Sauer B.** Inducible gene targeting in mice using the Cre/lox system. *Methods (Duluth)* 14: 381-392, 1998.

26. **Shiratori H and Hamada H.** The left-right axis in the mouse: from origin to morphology. *Development* 133: 2095-2104, 2006.

27. **Smith DJ, Gaffney EA, and Blake JR.** Modelling mucociliary clearance. *Respir Physiol Neurobiol* 163: 178-188, 2008.

28. **Storm van's Gravesande K and Omran H.** Primary ciliary dyskinesia: clinical presentation, diagnosis and genetics. *Annals of Medicine* 37: 439-449, 2005.

29. **Takaki E, Fujimoto M, Nakahari T, Yonemura S, Miyata Y, Hayashida N, Yamamoto K, Vallee RB, Mikuriya T, Sugahara K, Yamashita H, Inouye S, and Nakai A.** Heat shock transcription factor 1 is required for maintenance of ciliary beating in mice. *Journal of Biological Chemistry* 282: 37285-37292, 2007.

30. **Tan SY, Rosenthal J, Zhao XQ, Francis RJ, Chatterjee B, Sabol SL, Linask KL, Bracero L, Connelly PS, Daniels MP, Yu Q, Omran H, Leatherbury L, and Lo CW.** Heterotaxy and complex structural heart defects in a mutant mouse model of primary ciliary dyskinesia. *J Clin Invest* 117: 3742-3752, 2007.

31. **Toskala E, Smiley-Jewell SM, Wong VJ, King D, and Plopper CG.** Temporal and spatial distribution of ciliogenesis in the tracheobronchial airways of mice. *American Journal of Physiology - Lung Cellular & Molecular Physiology* 289: L454-459, 2005.

32. **Winters SL, Davis CW, and Boucher RC.** Mechanosensitivity of mouse tracheal ciliary beat frequency: roles for Ca2+, purinergic signaling, tonicity, and viscosity. *American Journal of Physiology - Lung Cellular & Molecular Physiology* 292: L614-624, 2007.

33. **Yu Q, Shen Y, Chatterjee B, Siegfried BH, Leatherbury L, Rosenthal J, Lucas JF, Wessels A, Spurney CF, Wu YJ, Kirby ML, Svenson K, and Lo CW.** ENU induced mutations causing congenital cardiovascular anomalies. *Development* 131: 6211-6223, 2004.

34. **Zhang Y, Huang G, Shornick LP, Roswit WT, Shipley JM, Brody SL, and Holtzman MJ.** A transgenic FOXJ1-Cre system for gene inactivation in ciliated epithelial cells. *American Journal of Respiratory Cell & Molecular Biology* 36: 515-519, 2007.

FIGURE LEGENDS

Figure 1. Postnatal increase in ciliation of the mouse tracheal epithelium.

(A-F). Fluorescent immunostaining of the trachea epithelium at PND 0-21 with Cy3 conjugated acetylated tubulin antibody delineated the cilia (red), while Alexa-Fluor 488 conjugated phalloidin delineated the outlines of individual epithelial cells (green).

(G) A linear relationship (R^2=0.9402) is observed between the percentage of ciliated tracheal epithelium cells versus age. Significant differences ($P<0.05$) were seen between time points unless otherwise marked as not significant (ns). Data presented as Mean ± SD. All scale bars =10 μm.

Figure 2. Measurement of cilia generated flow in the tracheal epithelium.

(A,B). DIC images of PND 0 (A) and PND 14 (B) tracheal epithelia viewed longitudinally.

(C,D). Fluorescent 0.20μm microspheres were added to the tracheal preparation and visualized under epifluorescent illumination. Video microscopy followed by tracing of the movement of four individual beads (1-4) in the two preparations.

(E,F). Cilia generated flow was quantified by analyzing the velocity (E) and directionality (F) of movement associated with the fluorescent microspheres. Significant differences ($P<0.001$) were seen between time points unless otherwise marked as not significant (ns). Data presented as Mean ± SD. All scale bars =10 μm.

Figure 3. Histograms of tracheal flow velocity and flow directionality.

The distribution of all microsphere speed and directionality measurements are shown (n= 48, 81, 101, 41, 51, 31, for PND 0, 3, 5, 7, 9, and 28 respectively). Note the broadening distribution of speed, while directionality plateaued to maximal flow directionality at PND 7.

Figure 4. Cilia waveform and beat frequencies in mouse tracheal epithelia.

(A,B). Shown are individual frames from movies obtained from PND 0 and PND 14 tracheal epithelia.

(C,D). Forward and return strokes traced from a single cilia beat cycle at PND 0.

(E, F). Forward and return strokes traced from a single cilia beat cycle at PND 14.

(G). CBF was quantified in trachea harvested from near term embryos (E18.5) and in mouse neonates between PND 0 - PND 28 in age. While the CBF in E18.5 embryo and PND 1-2 stage neonates was somewhat elevated compared to later stages, only the PND 0 CBF was significantly elevated compared to all other time points (* $P<0.001$). Data presented as mean ± SD. All scale bars =5 μm.

Figure 5. Ciliated cell abundance correlates with cilia generated flow in mouse tracheal epithelia.

The percentage of ciliated epithelial cells was plotted against flow speed (A) or directionality (B). Dotted-red lines are best fit for PND 0-28, and dotted green lines are best fit for PND 0-9. Directionality shows the best correlation with ciliated trachea

epithelia cell number during the initiation of cilia generated flow between PND 0-9 (R^2=0.975), while speed was less well correlated during this same time interval (R^2=0.495). Data presented as mean ± SD.

Figure 6. Airway epithelial cilia of *Mdnah5*$^{del267-859}$ mutants lack Mdnah5 protein and do not generate epithelial flow.

(A-D) Analysis of Mdnah5 expression in tracheal epithelial cells.

Immunostaining with a mouse monoclonal (A,B) or rabbit polyclonal (C,D) antibody to DNAH5 showed strong staining in the ciliary axoneme of wildtype (+/+) mice. However, the tracheal epithelial cells from homozygous *Mdnah5*$^{del267-859}$ mutants (m/m) displayed little or no staining in the ciliary axoneme. Specificity of the mouse monoclonal (A) and rabbit polyclonal (C) antibodies were shown with immunoblotting of extracts from airway epithelia, which showed a band of approximately 500 kd (arrows in A, C), the size range expected for Mdnah5. Scale bars = 5 μm.

(E,F). Quantitative analysis of cilia generated flow in *Mdnah5*$^{del267-859}$ mutants.

Cilia generated flow was quantified by analyzing the speed (E) and directionality (F) of movement associated with fluorescently labeled microspheres placed above the tracheal epithelia. In homozygous *Mdnah5*$^{del267-859}$ mutants (blue lines), both the speed and directionality were significantly different (denoted by asterisks) from control values (red lines). Data presented as mean ± SD.

(I). Cilia tracing of a forward and return stroke in *Mdnah5*$^{del267-859}$ mutant.

Tracing of a forward and reverse stroke of cilia from a *Mdnah5*$^{del267-859}$ mutant epithelial cell obtained using images obtained from a high speed (200 fps) movie. Note absence of

the characteristic sweeping motion normally seen in wild type airway cilia (Fig. 4C-F). Scale bar = 2 μm.

ONLINE DATA SUPPLEMENT LEGENDS

Supplemental Movie E1: Movie of cilia generated flow in a PND 0 trachea sample using 0.20μm fluorescent microspheres and epifluorescent microscopy. Movie collection and play back is 15 fps.

Supplemental Movie E2: Movie of cilia generated flow in a PND 14 trachea sample using 0.20μm fluorescent microspheres and epifluorescent microscopy. Movie collection and play back is 15 fps.

Supplemental Movie E3: DIC movie showing cilia beat shape observed in a PND 14 trachea sample. The movie was collected at 200 fps, while play back is 5 fps.

Supplemental Movie E4: DIC movie showing defective cilia motility in a *Dnahc5* homozygous mutant PND 14 trachea sample. Movie collection and play back is 15 fps.

Supplemental Movie E5: Movie of cilia generated flow in a *Dnahc5* homozygous mutant PND 14 trachea sample using 0.20μm fluorescent microspheres and epifluorescent microscopy. Movie collection and play back is 15 fps.

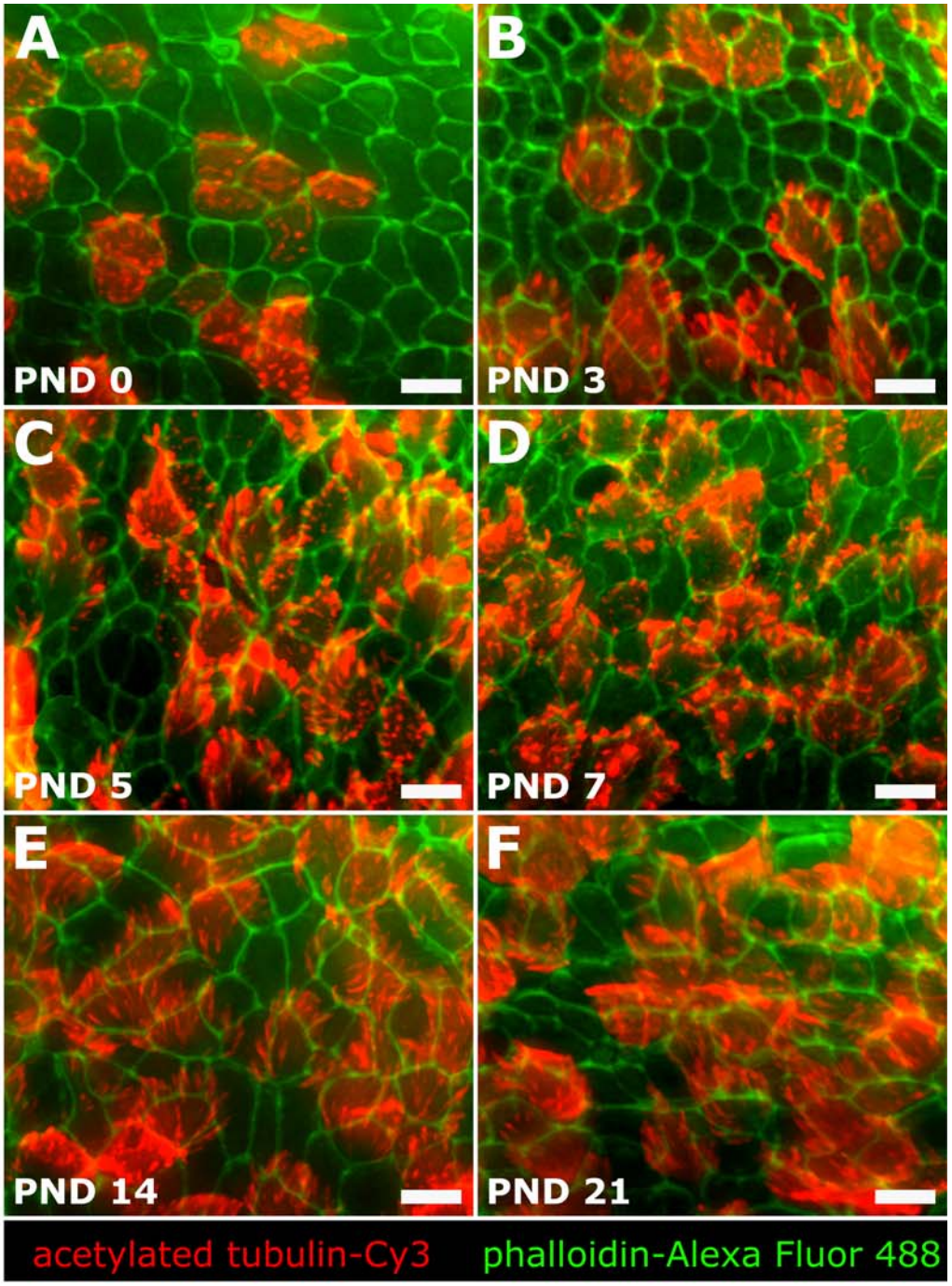
A
PND 0
B
PND 3
C
PND 5
D
PND 7
E
PND 14
F
PND 21
acetylated tubulin-Cy3
phalloidin-Alexa Fluor 488

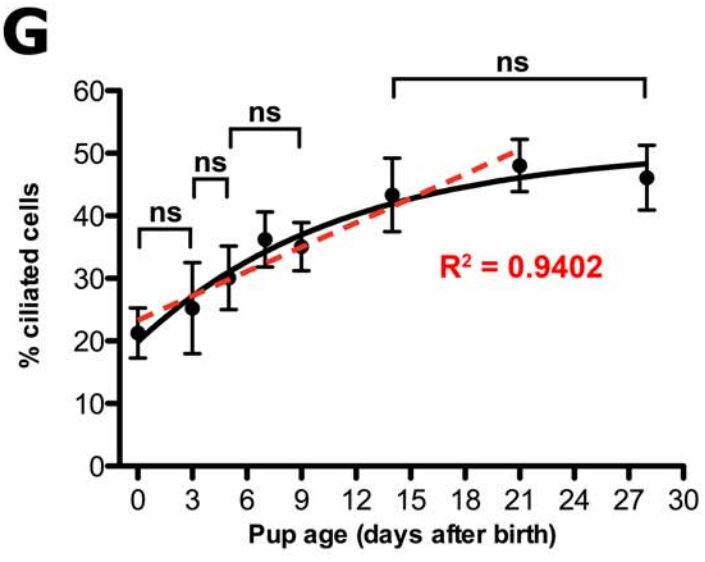
G
ns
ns
ns
ns
R² = 0.9402
% ciliated cells
0
10
20
30
40
50
60
0 3 6 9 12 15 18 21 24 27 30
Pup age (days after birth)

1

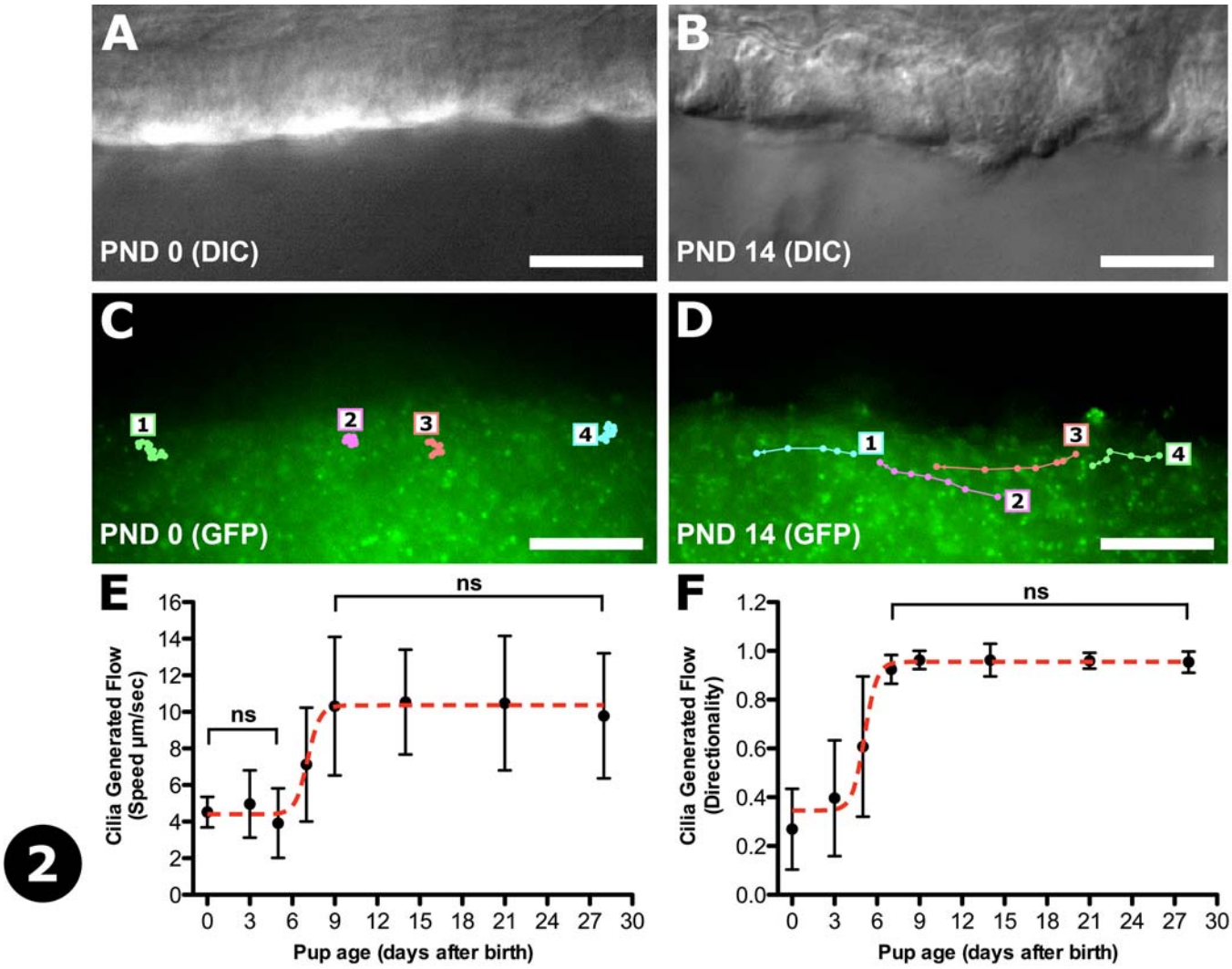
A
PND 0 (DIC)
B
PND 14 (DIC)
C
1
2
3
4
PND 0 (GFP)
D
1
2
3
4
PND 14 (GFP)
E
ns
ns
Cilia Generated Flow (Speed µm/sec)
0
2
4
6
8
10
12
14
16
0 3 6 9 12 15 18 21 24 27 30
Pup age (days after birth)
F
ns
Cilia Generated Flow (Directionality)
0.0
0.2
0.4
0.6
0.8
1.0
1.2
0 3 6 9 12 15 18 21 24 27 30
Pup age (days after birth)

2

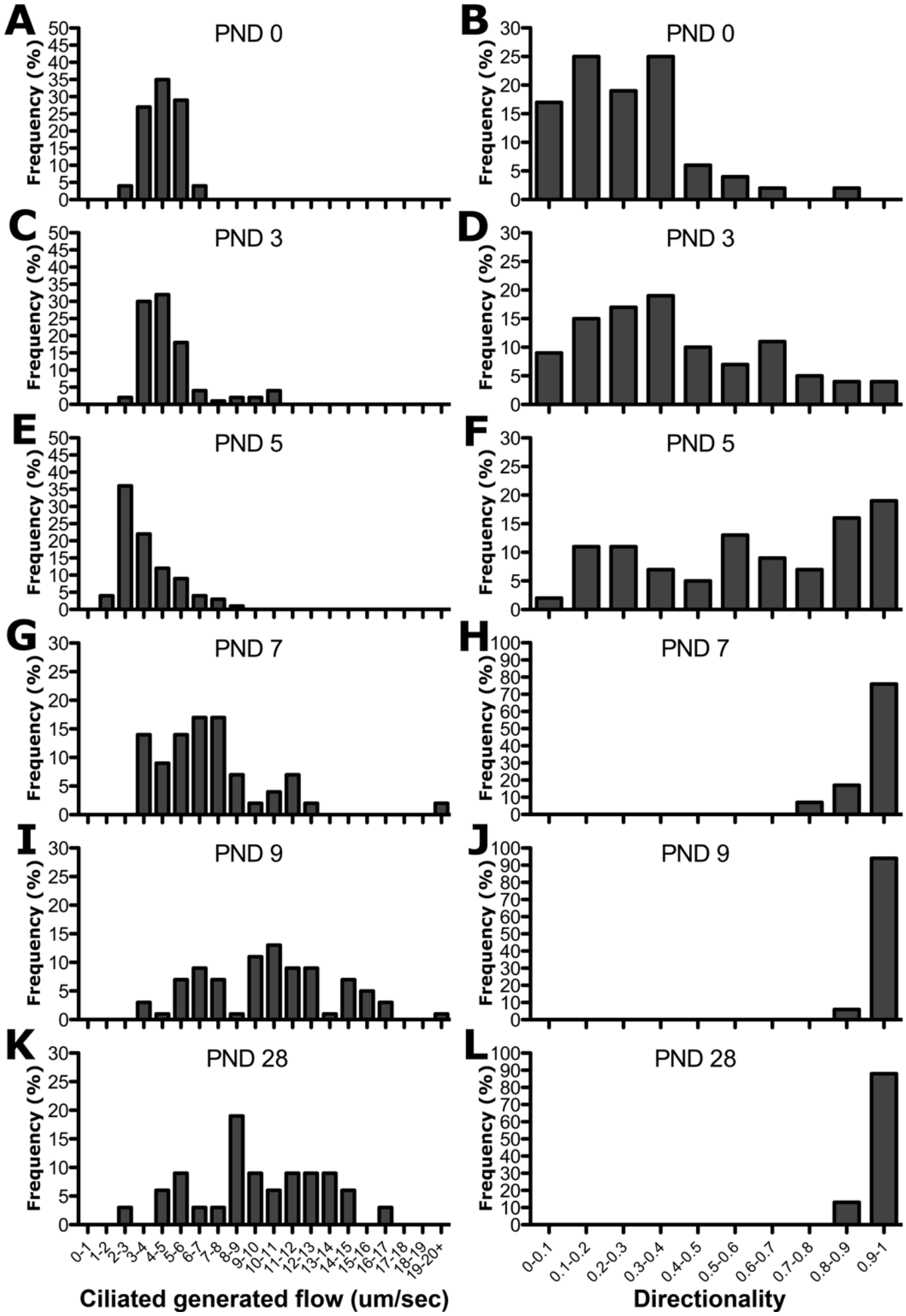
A
PND 0
B
PND 0
C
PND 3
D
PND 3
E
PND 5
F
PND 5
G
PND 7
H
PND 7
I
PND 9
J
PND 9
K
PND 28
L
PND 28
Frequency (%)
0-1
1-2
2-3
3-4
4-5
5-6
6-7
7-8
8-9
9-10
10-11
11-12
12-13
13-14
14-15
15-16
16-17
17-18
18-19
19-20+
Ciliated generated flow (um/sec)
0-0.1
0.1-0.2
0.2-0.3
0.3-0.4
0.4-0.5
0.5-0.6
0.6-0.7
0.7-0.8
0.8-0.9
0.9-1
Directionality

3

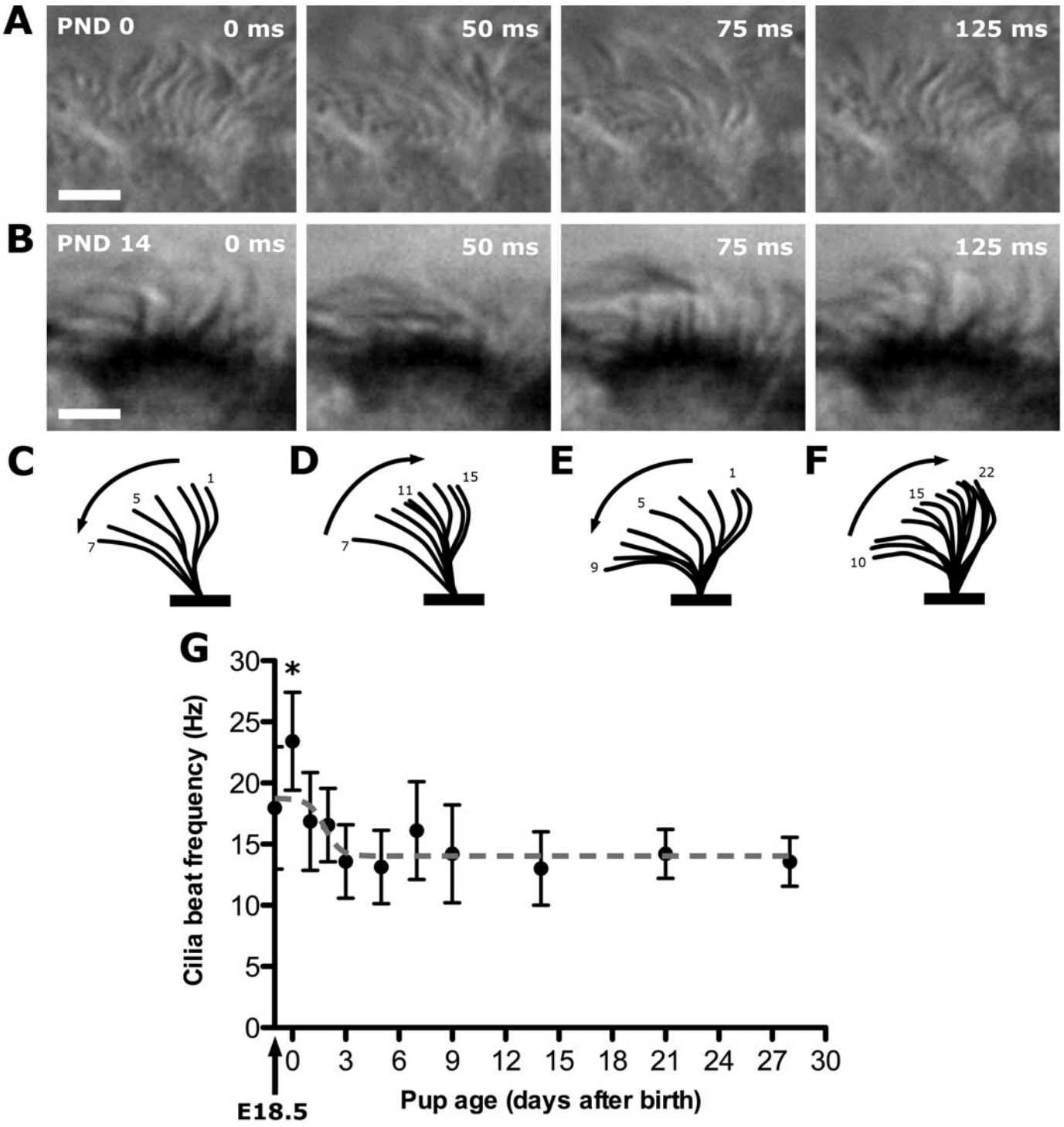
A
PND 0
0 ms
50 ms
75 ms
125 ms
B
PND 14
0 ms
50 ms
75 ms
125 ms
C
1
5
7
D
7
11
15
E
1
5
9
F
10
15
22
G
Cilia beat frequency (Hz)
30
25
20
15
10
5
0
*
0
3
6
9
12
15
18
21
24
27
30
E18.5
Pup age (days after birth)

4

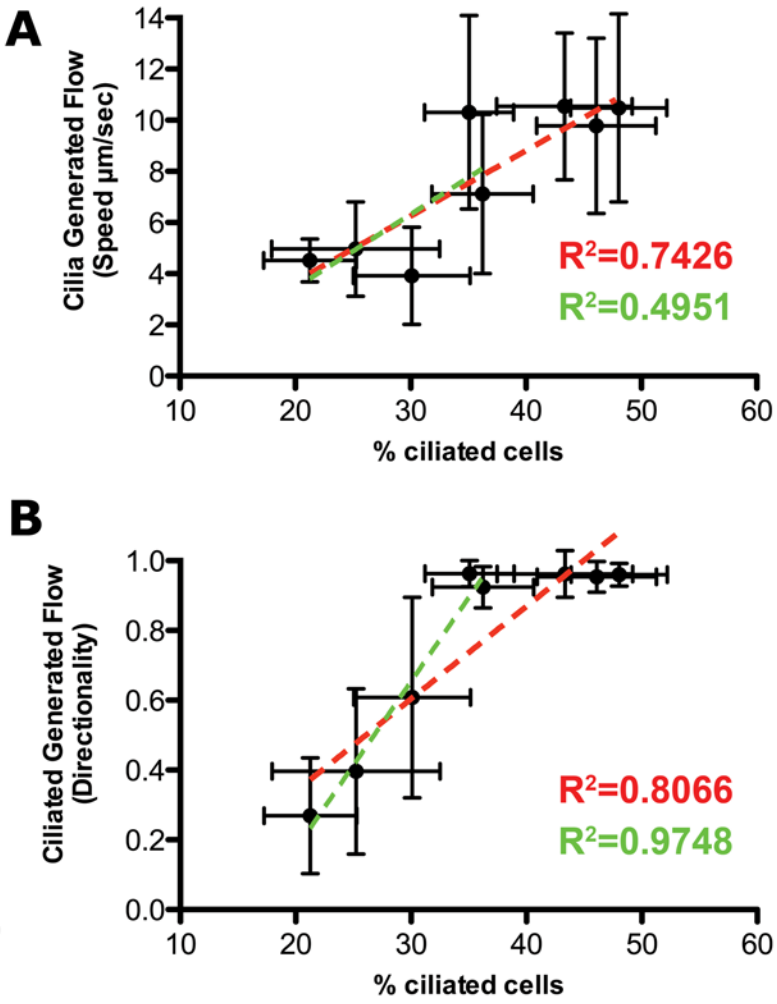
A
Cilia Generated Flow
(Speed µm/sec)
14
12
10
8
6
4
2
0
10
20
30
40
50
60
% ciliated cells
R²=0.7426
R²=0.4951
B
Ciliated Generated Flow
(Directionality)
1.0
0.8
0.6
0.4
0.2
0.0
10
20
30
40
50
60
% ciliated cells
R²=0.8066
R²=0.9748

5

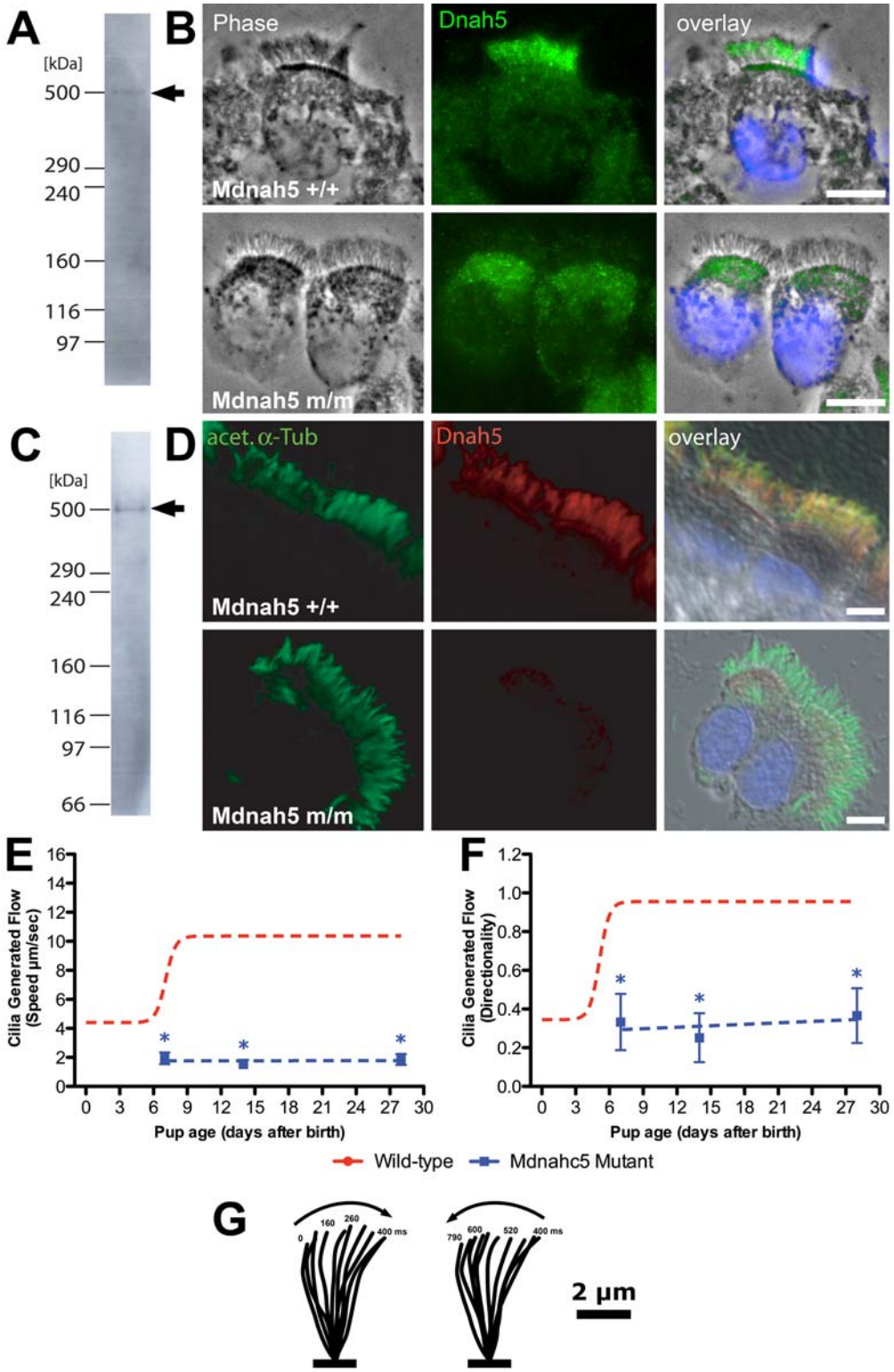
A
[kDa]
500
290
240
160
116
97
B
Phase
Dnah5
overlay
Mdnah5 +/+
Mdnah5 m/m
C
[kDa]
500
290
240
160
116
97
66
D
acet. α-Tub
Dnah5
overlay
Mdnah5 +/+
Mdnah5 m/m
E
Cilia Generated Flow (Speed µm/sec)
Pup age (days after birth)
F
Cilia Generated Flow (Directionality)
Pup age (days after birth)
Wild-type
Mdnahc5 Mutant
G
0
160
260
400 ms
790
600
520
400 ms
2 µm

6